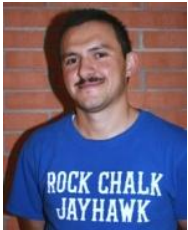


EVALUATION OF THE PERFORMANCE OF RETROFIT MEASURES FOR DISTORTION INDUCED FATIGUE USING FINITE ELEMENT ANALYSIS



TEMPLE RICHARDSON



FATIH ALEMDAR



CAROLINE BENNETT



ADOLFO MATAMOROS



STANLEY ROLFE

BIOGRAPHY

Temple Richardson is a Master's student at The University of Kansas. She also received her BSCE from the University of Kansas.

Dr. Fatih Alemdar is a recent PhD graduate from The University of Kansas, where he also received his MSCE.

Dr. Caroline Bennett is an Assistant Professor at The University of Kansas.

Dr. Adolfo Matamoros is an Associate Professor at The University of Kansas.

Dr. Stanley Rolfe is an Alfred P. Learned Distinguished Professor at The University of Kansas.

SUMMARY

This study focuses on evaluating retrofit measures for steel bridges with distortion-induced fatigue damage. Simulations using finite element models (FEA) were performed to analyze the complex stress field that develops in the web-gap region of bridge girders affected by distortion-induced fatigue.

Finite element models were calibrated with experimental results from 9-ft girder assemblies that were tested under fatigue loading. The calibrated models were used to evaluate the expected performance of various retrofit measures in terms of the effect of the retrofit measure on the stress demand and the potential for existing crack growth.

Retrofits studied include: crack-stop holes, tensioned bolts in crack-stop holes, back-up stiffeners, composite blocks, angles connecting the connection stiffener to top flange, and angles with a backing plate connecting the connection stiffener with the web.

EVALUATION OF THE PERFORMANCE OF RETROFIT MEASURES FOR DISTORTION INDUCED FATIGUE USING FINITE ELEMENT ANALYSIS

Abstract

Many existing steel girder bridges designed prior to the mid-1980s were fabricated leaving a flexible gap in the girder web, between the connection plate of transverse cross frames and the girder flange. These flexible web gaps are susceptible to out-of-plane distortion damage due to transverse forces induced by cross-frame forces when the adjacent girder is subjected to a larger deflection. Various retrofit measures have been developed to address this problem including the drilling of crack-stop holes, installation of tensioned bolts, use of composite materials, back-up stiffeners, and installation of steel angles to directly transfer the forces from the connection plate to the flange. All these measures are intended to reduce the rate of growth of the cracks and to prevent the further initiation of cracks.

This study focuses on evaluating retrofit measures for steel bridges with distortion-induced fatigue damage. Simulations using finite element models (FEM) were performed to analyze the complex stress field that develops in the web-gap region of bridge girders affected by distortion-induced fatigue. The Extended Finite Element Method (XFEM) was used to study the stress field in the web-gap regions of girders with existing fatigue cracks and the potential for crack growth after a retrofit measure has been installed.

Finite element models created using ABAQUS 6.10 were calibrated with experimental results from 9-ft girder assemblies that were tested under fatigue loading. The calibrated models were used to evaluate the expected performance of various retrofit measures in terms of the effect of the retrofit measure on stresses and the potential for existing crack growth.

Simulation results show that two newly developed retrofit measures utilizing composite materials and attaching steel angles to the connection plate and web of the girder were the most effective in reducing the potential for further fatigue damage.

Introduction

Background

Damage due to distortion-induced fatigue is a problem commonly found in structural steel bridges built prior to the mid-1980s. This type of fatigue damage often occurs in cross-frame-to-girder connections, in an area called the web gap region, and is caused by the action of secondary stresses neglected during the original design of the structure. A web gap can be described as a short length of a girder web bounded on one end by the girder flange and on the other by the termination of the cross-frame connection stiffener. When the connection stiffener is not attached to the girder flange, a short flexible segment of girder web is created between the connection stiffener and the girder flange that must transfer the out-of-plane forces induced in the cross frame to the slab or girder flange. The problem is exacerbated by the presence of geometric discontinuities that give rise to stress concentrations in this region of the girder. Two locations in the web gap that are particularly vulnerable to fatigue damage are the connection stiffener-to-web weld and the flange-to-web weld. The combination of high stress and geometric discontinuities in these two locations often leads to the formation of fatigue cracks.

When secondary stresses lead to cracking in the web gap region, bridge engineers are faced with designing an appropriate retrofit measure to completely halt crack propagation or at least reduce the rate of crack growth so the fatigue life of the bridge can be extended while other options are pursued. A “toolkit” of existing retrofit techniques for distortion-induced fatigue are currently available for this purpose, including drilling crack-stop holes; stiffening the web gap region by providing a direct connection of the stiffener with the flange; and softening the web gap region through removal of material from the connection stiffener.

The most common measure applied to bridges with fatigue cracks consists of drilling crack-stop holes at the tips of cracks. This technique is intended to eliminate the sharp termination of the crack and replace it with a smooth radius, lowering crack growth propensity by reducing the stress-concentration factor. Expressions to calculate the diameter of crack-stop holes have been proposed (1) based on experimental results from steel plates subjected to in-plane stresses (Eq. 1).

$$\frac{\Delta K}{\sqrt{\rho}} < 10\sqrt{\sigma_y} \quad (\text{Eq.1})$$

In Eq. 1 the crack-stop hole diameter, ρ , depends on the stress intensity factor, K , and the yield strength of the material, σ_y . Although Eq. 1 was not developed for out-of-plane fatigue loading (1), crack-stop holes proportioned with this equation are often employed to temporarily halt the propagation of fatigue cracks caused by distortion-induced fatigue because the drilling of the hole serves to eliminate the sharp tip at the end of the crack. When cracks re-initiate and continue to propagate, more holes are drilled, resulting in a progressive weakening of the web gap region. In a study performed by Fisher (2), the diameter of crack stop holes varied from 19 to 76 mm (0.75 to 3 in.).

Roddis and Zhao (3) performed high-resolution computer simulations to compare the relative performance of introducing a slot in the connection stiffener, intended to reduce the stress at the web gap by making the cross-frame-to-girder connection more flexible, and a retrofit measure consisting of welding the connection stiffener to the compression flange, which reduces the stress at the web gap by adding connectivity between the stiffener and the flange. In the case study presented the authors concluded that the slotting retrofit measure was ineffective, and a final repair was recommended in which the connection stiffener was welded to the compression flanges. While the geometry of the slot used by Roddis and Zhao (3) could have been modified following the recommendations by Fisher (2) to improve its effectiveness, FE results showed that the reduction in stress at the web gap region associated with creating connectivity between the stiffener and the flange was indicative of excellent performance.

Not all retrofit measures that rely on stiffening of the connection lead to the same outcome. For example, welding a connection plate to a tension flange introduces a fatigue-vulnerable detail that may allow for reinitiation of a fatigue crack and propagation into a flange. To avoid this type of damage, many State Departments of Transportations (DOTs) have implemented a repair that consists of adding connectivity by bolting double angles to the connection stiffener and the flange. In cases where the fatigue damage is at the top of the web, this procedure can require removal of a concrete deck, which is costly and requires traffic disruptions. An alternative similar retrofit involves welding the head of a bolt or piece of threaded rod to the inside face of the flange, which allows bolting the flange to the connection stiffener without removal of the deck. The main drawback of this technique is that it may introduce a fatigue-vulnerable connection at the weld between the threaded rod and the flange. Given the challenges inherent to the repair of distortion-induced fatigue damage there is a clear and immediate need to develop retrofit measures that are cost-effective, easy to install, minimize the disruptions to ongoing traffic, and most importantly, can be effective without introducing new vulnerabilities to fatigue damage as a “side effect”.

Objective

The objective of this study was to evaluate the performance of several retrofit measures for distortion-induced fatigue in steel bridge girders based on analyses of high-resolution 3D finite element models and tests of physical specimens. The scope of this study included examining distortion-induced fatigue in the web gap region of a steel bridge girder with non-skewed cross-frames. The retrofits were primarily examined with the goal of identifying their effectiveness in cracked girder geometry, with the exception of the transverse back-up stiffener and web-to-stiffener angles and backing plate retrofits, which were examined in both cracked and uncracked configurations.

Research Approach

A two-pronged approach was adopted in this research. A coordinated study was performed simultaneously using (1) detailed 3D FEA and (2) physical testing of steel girders under distortion-induced fatigue loads. The two research techniques were used in a complementary manner. For example, results from FEA aided in determining the locations of the physical specimens that were most susceptible to distortion-induced fatigue damage, and also provided a basis for evaluating the relative performance of the various retrofit techniques. Measurements from the physical specimens were used to calibrate the FE model, so that model characteristics such as the boundary conditions and the mesh density could be refined to best represent the test environment. To adequately describe the coordinated effort, some information concerning the approach is necessary.

Experimental Test Set-up

The test specimens were proportioned such that they were each 2,845-mm (112-in.) long with web dimensions of 876×10 mm ($34.5 \times 3/8$ in.). The width of the top and bottom flanges was 279 mm (11 in.), with the top flange having a thickness of 25 mm (1.0 in.) and the bottom flange width being 16 mm ($5/8$ in.). In the physical model, the girder specimen was connected to the laboratory floor through a series of channels post-tensioned to the concrete floor, as shown in Figures 1 and 2. The girder was tested upside-down, with the laboratory floor simulating the restraint offered by a concrete bridge deck. The top flange in the laboratory model (*top flange_{test}*) reflected behavior for a discretely braced bottom flange in a bridge girder (*bottom flange_{bridge}*). The top flange_{test} was restrained at both ends in the out-of-plane direction by angles connected back to a stiff anchorage (a channel member on the load frame), to simulate the restraint effects provided by intermediate cross-frames and lateral flange bending resistance of the bottom flange_(bridge). Full-depth stiffeners were provided at the girder ends to ensure web stability in those regions.



Figure 1. View of of girder specimen



Figure 2. View of fascia side of girder specimen

The specimen was tested cyclically using load control, with the actuator applying a tensile force with a maximum load of 205 kN (4.6 kips) and a minimum of 356 kN (0.8 kip). The load was applied to the specimen through an assemblage comprised of a WT section which was directly connected to the actuator at the top, and directly connected to the cross-frame members.

Finite Element Analysis Approach

The specimen and loading apparatus were modeled closely, as shown in Figures 3 and 4, using the commercially-available FEA software ABAQUS v6.10. The concrete laboratory floor and the girder tie-down system were simulated in the models. Movement of the actuator in the lateral or longitudinal direction of the girder was prevented. In the simulation, the loading step was divided into five increments, with a static load of 5 kips.

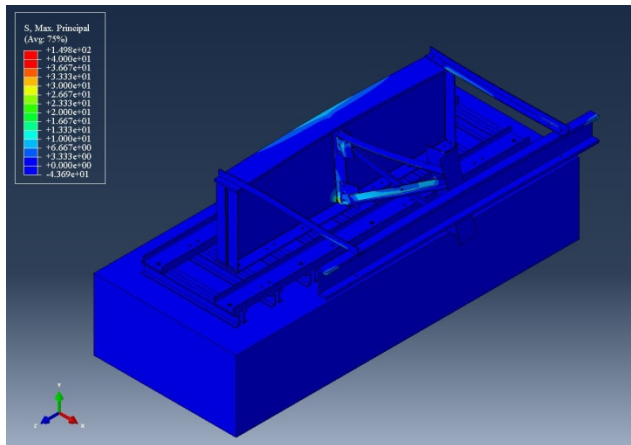


Figure 3. Overall view of girder FE model

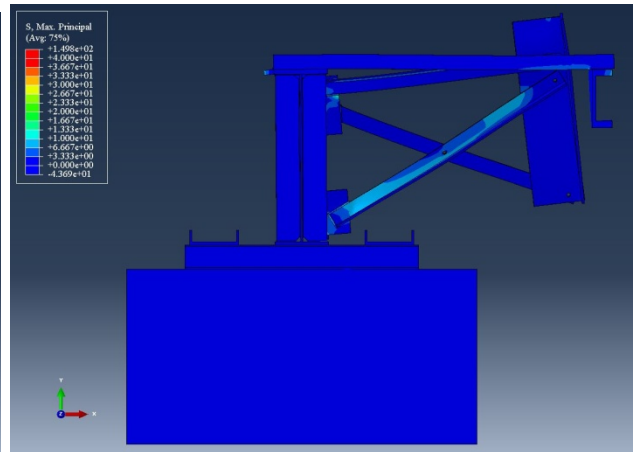


Figure 4. Cross-section view of girder FE model

Table 1. Material properties used in FE model

Material	Modulus of Elasticity, [MPa (ksi)]	Poisson's ratio
Steel	200,000 (29,000)	0.3
Concrete	27,800 (4,030)	0.2
Carbon fiber reinforced polymer (CFRP)	Varied between 34,500 – 69,000 (5,000 – 10,000)	0.1

The mesh in the web was determined based on the proximity to the web gap region. The mesh near this region was very dense, with eight-node brick elements sized at 2.54 mm (0.1 in.). Further away from the web gap region the mesh size was 9.53 mm ($\frac{3}{8}$ in.). Tetrahedral elements were used to transition between these mesh sizes. Welds also contained hexagonal eight-node brick elements, and were modeled as right triangles. The mesh element size for welds was 2.54 mm (0.1 in.). Tie constraints were used to connect welds to the web and flanges and the cross-braces to the gusset plates. The number of degrees of freedom in each model varied depending on crack placement and retrofit configuration, and varied from 1 million to 2.5 million degrees of freedom.

Bolts were modeled explicitly, and were composed of three merged parts: the shank, nut, and head. The middle of the shank was partitioned so that a bolt load could be applied to the interior face. The head and shank of the bolt were connected to structural elements using tie constraints. The bolt load was determined based on the recommendations in the AISC Steel Construction Manual (4) based on the specific diameter of the bolt that was used. Bolt tensioning forces were applied in the second loading step of the computer simulations. The actuator load was applied in the third loading step. Although the applied bolt load was removed in this step, the tension force was maintained by keeping the contracted bolt length at the end of the second loading step constant for all subsequent steps. This technique greatly simplified the model and decreased the numerical complexity of the solution, yet still accounted for the tension force in the bolts. In other areas, such as the channels connected to the bottom flange in the test set-up (bottom flange_{test}), bolts were not modeled. Instead, the channels were tied to the bottom flange_{test}. In areas of greater interest, such as the bottom web gap_{test}, actual bolts were modeled explicitly.

Three different techniques for modeling cracks were utilized: explicit modeling of the cracks, the Extended Finite Element Method (XFEM), and contour integrals. Differences in the characteristics of the models and the types of outputs that were needed dictated the selection of the crack modeling technique.

Cracks were modeled explicitly by removing elements from the web. Crack width was dependent upon the mesh density, so the mesh in the web gap region was set to 0.6 mm (0.02 in.) initially. The run time was longer than average in these models because the mesh was required to be very dense.

Cracks were also simulated through the use of the Extended Finite Element Method (XFEM). A major benefit of this numerical method over explicitly modeling cracks is that the finite element mesh is independent of the crack geometry. This can be advantageous when a crack is allowed to propagate in the XFEM simulation, and also because the crack does not need to align with element boundaries. Enrichment functions are added to the approximation space near crack tips (5). In XFEM simulations, the part containing a crack was partitioned such that the area around the crack tip could be selected for enrichment. When a fixed area around the crack tip was enriched, as opposed to just the nodes around the crack tip, the rate of convergence was greatly increased (5).

In the retrofits examined, a crack with a predefined length and no propagation was used for retrofit comparison. In the XFEM simulations, cracks were modeled as 3D planar parts and the depth of the crack was set to the thickness of the web, 9.5 mm ($\frac{3}{8}$ in.). One of the limitations of the XFEM technique was that in many instances, when cracks intersected a boundary between model parts, the elements became distorted and the cracks did not open. This limitation was overcome by placing the cracks a very

small distance, 0.25 mm (0.01 in.), away from the part boundary. Enrichment functions could not be added to a crack tip that is located where elements are not present. An example of this situation is a crack truncating into a crack-stop hole. In this situation, explicit cracks were modeled in place of the XFEM technique. When using XFEM, J-Integral values could be obtained from each crack. J-integral results have been presented alongside HSS results for Retrofit 6, discussed in the Results section.

Finally, cracks were also simulated and analyzed using contour integrals. This technique was implemented to calculate contour integrals in the area surrounding the tip of the cracks, such as the J -integral, to be used as a measure of the potential for crack re-initiation in models with retrofit measures. When this method was used, the web was partitioned to have a small circle at each crack tip. The diameter of the circle was 5.1 mm (0.2 in.). The direction of crack growth was specified by the q -vector, defined in terms of the starting point of the crack and the crack tip. For cracks below the connection plate two q -vectors were specified, allowing both crack tips to grow. After the q -vector was defined, a seam was placed in the web which functioned as the crack. The q -vector was defined to act in the direction of the cracking paths noted in Figure 5a.

Evaluation of Crack Growth Propensity and Retrofit Effectiveness

When examining FE simulation results, it is important to use meaningful comparative measures of stress between models. Using maximum stresses as the measure for comparison is likely to provide an inaccurate comparison because it is sensitive to mesh size, particularly in areas of web gap regions with very large stress gradients.

Hot spot stress technique

The Hot Spot Stress (HSS) technique was used to quantify the stress near welds and geometric discontinuities. The two welds of particular interest were the connection stiffener-to-web weld and the web-to-bottom flange_(test) weld. Two hot spot stress paths were defined to capture maximum principal stresses in the regions directly surrounding those two welds. The paths were located half the thickness of the web away from each of the welds, and maximum principal stresses were extracted from each element on the path. The greatest maximum principal stress from each path was selected as the basis of comparison with HSS from other models. The magnitudes of the stresses obtained using the HSS techniques are sensitive to mesh size and the distance between the point of extraction of the stress and the weld toe. A convergence study was performed to determine the appropriate mesh size in the web gap region. Based on this study, the mesh size of the web in the web gap region was set to 2.54 mm (0.1 in.).

Two different hot spot stress paths were considered in this study: HSS1 and HSS2. When a crack along the stiffener-to-web weld toe was modeled (referred to as a *horseshoe-shaped crack*), the HSS path used was labeled HSS1. The HSS1 path was defined at a distance of half the thickness of the web away from the weld toe, but the path was always parallel to the crack geometry. If a crack was present along the toe of the weld connecting the web to the flange (referred to herein as a *horizontal crack*), a HSS path was taken 5 mm (0.2 in.) away from the weld toe (in the web), parallel to the crack. Paths taken parallel to a crack in the web-to-flange weld were labeled HSS2.

Figure 5a presents the location of the cracks modeled, and Figure 5b shows the two HSS paths considered in the bottom web gap_(test). In scenarios where crack length was varied, cracks were symmetric about mid-thickness of the stiffener. When comparing retrofits with varying crack lengths, the HSS path lengths were always kept constant. Therefore, the length of HSS2 was maintained at 203 mm (8 in.) and the height of HSS1 maintained at 102 mm (4 in.), regardless of the crack length examined. This approach allowed for the maximum principal stresses to be extracted for every element along the two paths in the various models; the reported HSS value for each path always corresponded to the greatest value of maximum principal stress along that path for the model being examined.

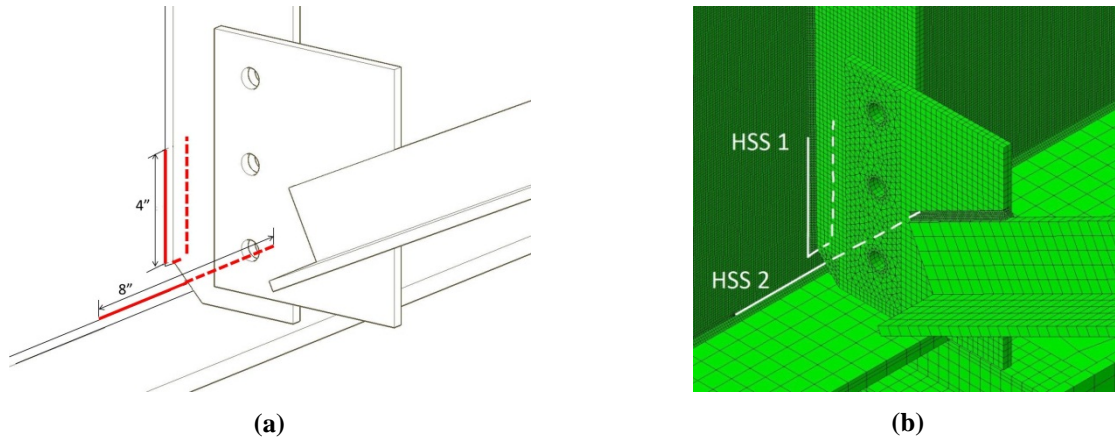


Figure 5. (a) Diagram of modeled 4-in. long horseshoe-shaped crack and 8-in. long horizontal crack geometry at weld toes; redlines represent modeled cracks.; (b) Location of HSS extraction paths, HSS1 and HSS2, in the bottom web gap_(test)

***J*-Integral**

The *J*-Integral is a path-independent contour integral that captures the energy released from a crack when it grows (7). It estimates the energy released at the crack tip by selecting a path a certain distance away from the assumed inelastic region present around the crack tip. In some models, it was found that the *J*-Integral was better suited than the Hot Spot Stress (HSS) technique for comparing the effectiveness of different retrofit measures because in some models the mesh had to be redefined to accommodate the retrofit measure. For example, the web mesh had to be redefined for angle-retrofit measures that required bolt holes. When *J*-Integral values were calculated, the contour integrals were defined at the tip of the crack. Five contour integrals were defined at planes that intersected the crack at different points through the thickness of the web, and *J*-Integral values were extracted from the plane located on the tension face of the web. *J*-Integrals from the fifth contour were used for comparison because the energy tends to converge with increasing number of contours.

ABAQUS calculates the *J*-integral in two ways. The first is by direct computation using well-established equations (1). The second is by calculating the *J*-Integral on the basis of the stress-intensity factors. In the web gap region where multiple crack surface displacements are possible (Modes I, II, and III), Equation 2 was used:

$$J = \frac{1}{E} (K_I^2 + K_{II}^2) + \frac{1}{2G} (K_{III}^2) \quad (\text{Equation 2})$$

where K_I , K_{II} , and K_{III} are stress intensity factors corresponding to Mode I, II, and III displacements, $E' = E/(1-\nu^2)$ for plane strain, E is Young's modulus, ν is Poisson's ratio, and G is the shear modulus (7).

Experimental Results

Two specimens, designated Specimen 1 and Specimen 2, were tested in the structures laboratory at the University of Kansas. The results from these two tests are discussed in the following.

Crack initiation/growth sequence

In the first specimen (Specimen 1), a 38-mm (1.5-in.) long crack was fabricated 20 mm (0.8 in.) below the connection stiffener-to-web weld. The intent of fabricating a crack prior to loading was to control the location and length of cracks at the start of the tests. Contrary to what was expected, the crack tips grew down towards the web-to-flange weld at the bottom flange_(test), and a second crack quickly initiated at the connection stiffener-to-web weld. Figures 6 and 7 present the simulation results for Specimen 1, with the experimentally-observed cracking superimposed. It can be readily observed that excellent agreement was observed between the maximum principal stresses calculated with the finite element model and the experimentally observed crack locations. It should be noted that the connection stiffener was removed from view in Figure 7.

Based on the findings from the first physical test, no pre-existing cracks were fabricated in Specimen 2. The first crack that formed in Specimen 2 was found at the connection stiffener-to-web weld. After the formation of this crack, the bottom flange_(test)-to-web weld developed a horizontal crack that quickly propagated.

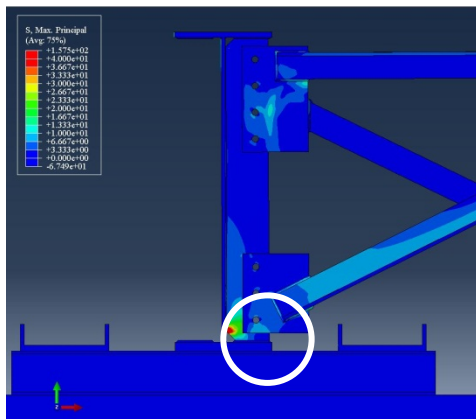


Figure 6. Overall view of specimen, with bottom web gap_(test) shown by the circle.

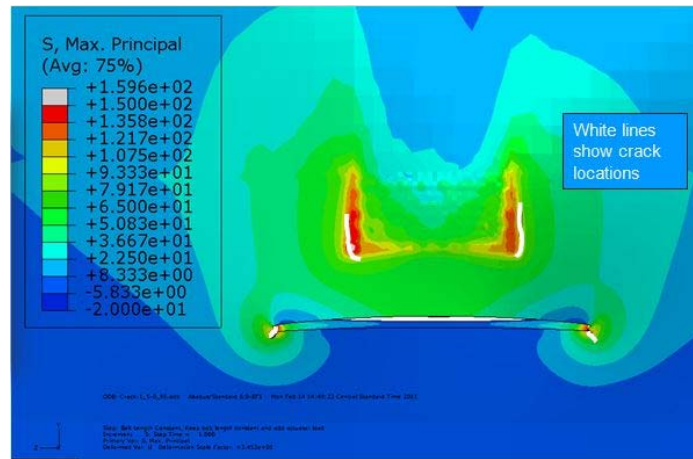


Figure 7. View of maximum principal stress contours in the cracked web gap region in the finite element model of Specimen 1. Superimposed white lines represent experimentally-observed cracks locations.

Finite Element Analysis Results

Unretrofitted Performance

In simulations of unretrofitted, uncracked models very high stresses were found at the toe of the weld between the web and the connection plate (Figures 8a and 8b). On the fascia side of the girder, in the bottom web gap of the specimen, an area of high stress was found at the web-to-bottom flange_(test) weld. Cracks formed in both of these areas in the bottom web gap during the experiment. In Specimen 2, horseshoe-shaped cracks first formed at the toe of the connection stiffener-to-web weld, followed by cracks at the web-to-bottom flange_(test) weld. The experimentally-observed crack pattern was in close agreement with locations of peak maximum principal stress calculated with the FE models. In Specimen 2, the horseshoe-shaped and horizontal cracks were allowed to grow to 102 mm (4 in.) and 203 mm (8 in.), respectively. This particular crack configuration was modeled, and increases of 4.5× and 25× were calculated for the magnitudes of HSS1 and HSS2, respectively, when compared with computed values from the uncracked configuration.

A small region of high stress was also noted in the top web gap on the fascia side of the web during simulations of unretrofitted specimens. During the test of Specimen 2, cracks were observed in the top web gap_(test) after cracks had initiated and propagated in the bottom web gap_(test).

Retrofit Measures

A series of retrofit measures were investigated analytically, some of which were also investigated experimentally. Retrofit measures discussed herein include (1) use of crack-stop holes, (2) installation of tensioned bolts in crack-stop holes, (3) use of transverse back-up stiffeners, (4) composite blocks, (5) bolted angles connecting the stiffener to the bottom flange_(test), and (6) bolted angles connecting the stiffener to the web along with a steel backing plate. Of these techniques, retrofit measures (1) and (6) were also applied to test specimens. All techniques are addressed in the following discussion.

Retrofit Measure 1: Crack-Stop Holes

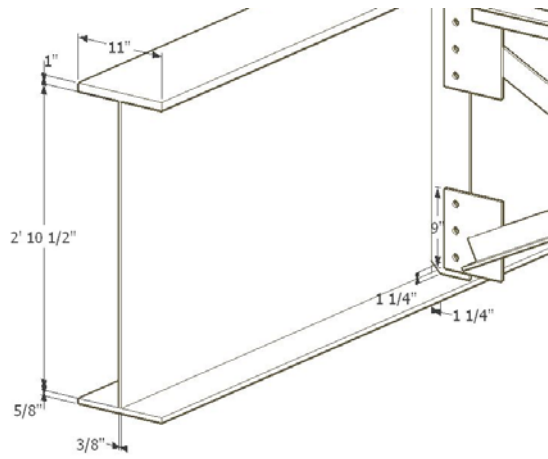
Retrofit measure 1 was studied both analytically and experimentally. In the physical Specimen 2, two 19 mm (³/₄ in.) diameter crack-stop holes were drilled at the tips of the 102-mm (4-in.) horseshoe-shaped crack along the connection plate weld and also at the tips of the 203-mm (8-in.) horizontal crack along the bottom flange weld. The holes were drilled as close to the crack tips as possible to remove the sharp crack tip. In some cases, portions of the connection plate-to-web weld had to be removed to achieve this end result.

This retrofit measure was modeled in the simulations, and is shown in Figures 9a and 9b. Cracks were modeled explicitly with a thickness equal to one element width, which was set to 2.54 mm (0.1 in.). The stress distribution in Figure 9b shows that there were very high stresses in the immediate vicinity of the crack stop holes, along the connection stiffener weld. The calculated value of HSS1 decreased by 38% after the holes were drilled. Although the reduction in the stress was meaningful for HSS 1, the calculated stress in the model without the crack stop holes was so high that the reduction in stress was not expected to prevent cracks from re-initiating.

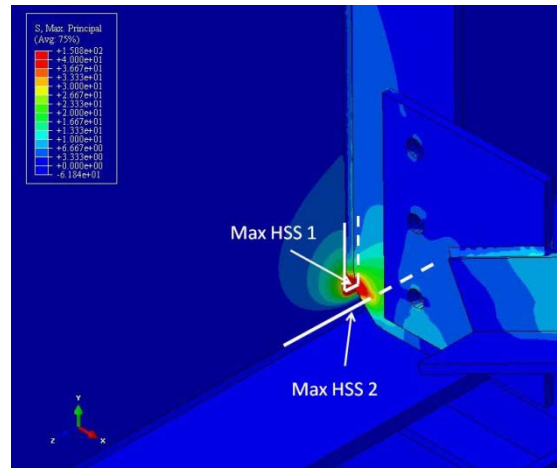
In Specimen 2, cracks indeed re-initiated a relatively small number of cycles after the holes were drilled, which was in agreement with results from the computer simulations. The length of the horseshoe-shaped crack before the crack-stop holes were drilled was 102 mm (4 in.), and after the holes were drilled, the horseshoe-shaped crack grew to 70 mm (2.75 in.) in 39,700 cycles. A photograph depicting the crack pattern and crack-stop hole placement is provided in Figure 9c.

Retrofit Measure 2: Tensioned Bolts and Square Washers

Retrofit measure 2 was studied analytically. In this case 19-mm (³/₄in.) diameter tensioned bolts were inserted into the crack-stop holes with the intent of applying a compressive stress to the crack tip. A view of this retrofit on the fascia and interior of the web is shown in Figure 10. In addition to tensioned bolts, 25 × 25-mm (1 × 1-in.) square washers were added to the fascia side of the web to investigate if the compressive stress could be distributed over a larger area. It was found that neither method significantly reduced the stress at the connection stiffener-to-web weld. Also, it should be noted that this type of retrofit is not possible to construct for all crack configurations because a bolt cannot always fit in geometrically constrained areas. In these simulations, this retrofit was possible only when the crack was at least 38 mm (1.5 in.) below the weld toe.

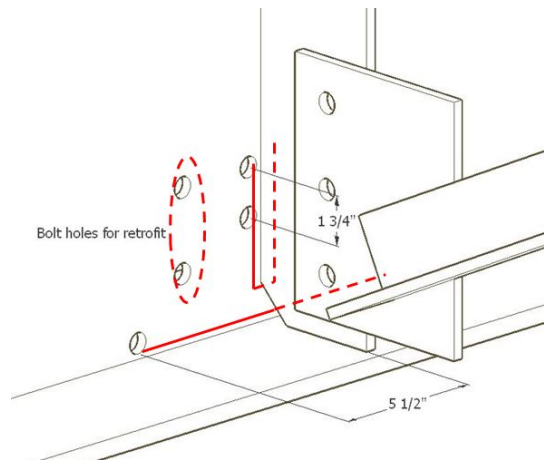


(a)

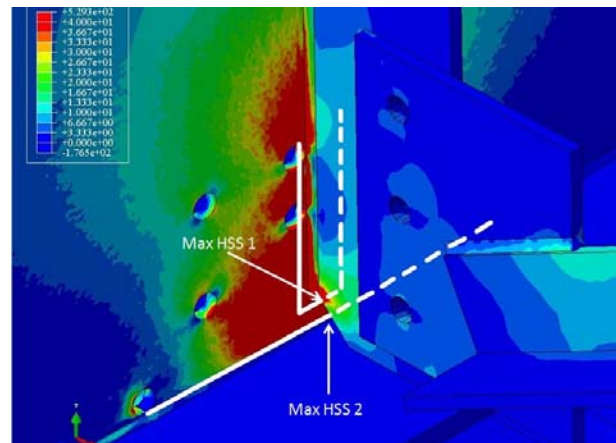


(b)

Figure 8. (a) Schematic of unretrofitted web gap region; (b) Maximum principal stress contour plot for unretrofitted web gap region (no cracks modeled); arrows point to point of highest maximum principal stress along HSS Paths 1 and 2.



(a)



(b)



(c)

Figure 9: Retrofit measure 1: drilled crack-stop holes (a) Schematic of drilled crack-stop holes, where redlines represent hot spot paths; (b) Maximum principal stress contour plot (cracks modeled explicitly); arrows point to point of highest maximum principal stress along HSS Paths 1 and 2; (c) Photograph of cracking pattern on fascia side of girder. Horseshoe-shaped cracking is visible, horizontal crack has been

highlighted in yellow.

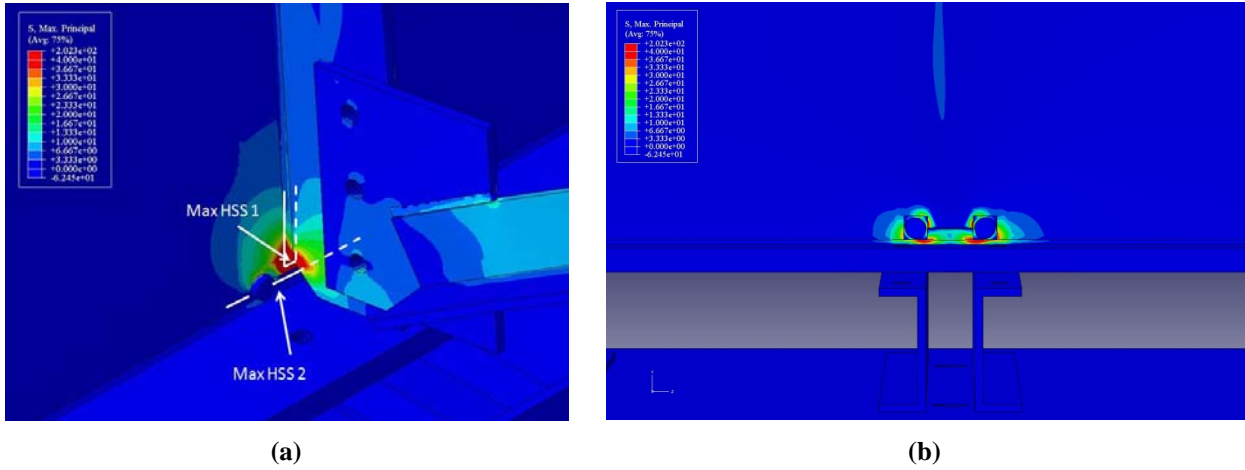


Figure 10. Retrofit measure 2: Tensioned bolts (a) view of stress contour plot for interior face of girder; (b) view of maximum principal stress contour plot for fascia side of girder; cracks modeled explicitly; arrows point to point of highest maximum principal stress along HSS Paths 1 and 2.

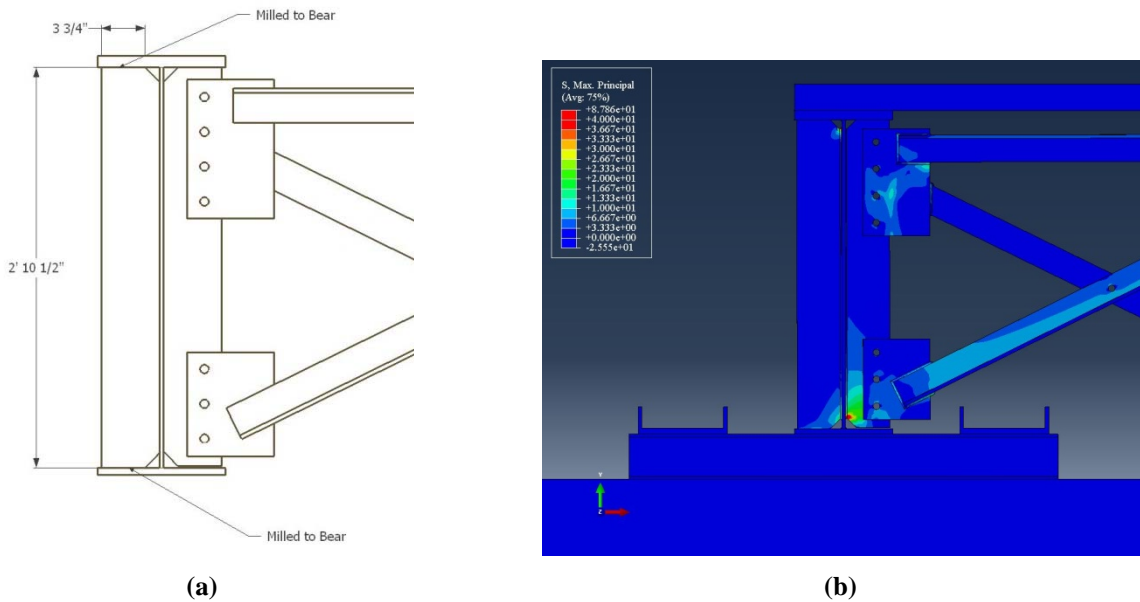


Figure 11. Retrofit measure 3a: (a) Schematic of full-depth transverse back-up stiffener; (b) Maximum principal stress contour plot for full-depth transverse back-up stiffener; cracks modeled using XFEM

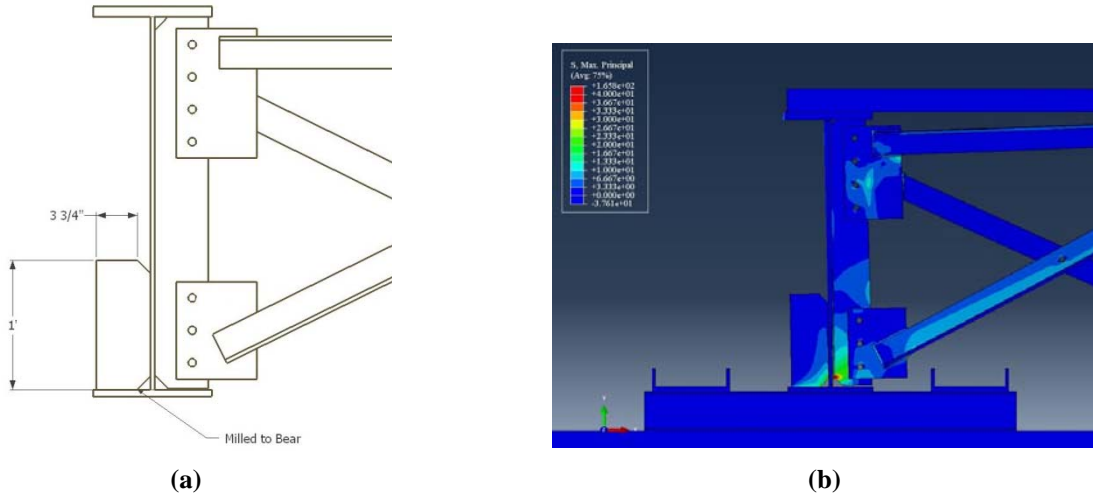


Figure 12. Retrofit measure 3b: (a) Schematic of partial-depth transverse back-up stiffener; (b) Maximum principal stress contour plot for 305-mm (12-in.) partial-depth transverse back-up stiffener; cracks modeled using XFEM

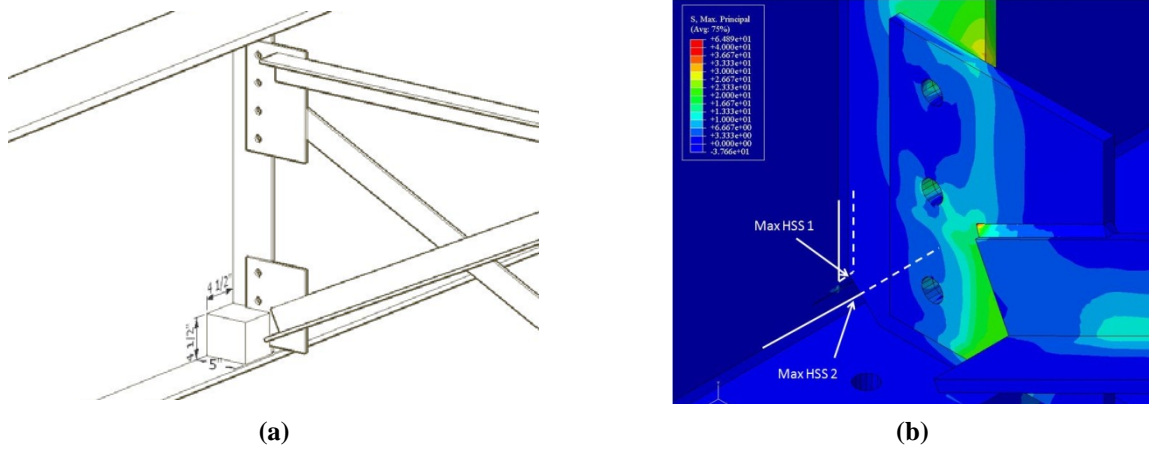


Figure 13. Retrofit measure 4: (a) Schematic of modeled geometry for the CFRP block (b) Maximum principal stress contour plot for steel beneath composite block; Cracks modeled explicitly. Arrows point to point of highest maximum principal stress along HSS Paths 1 and 2.

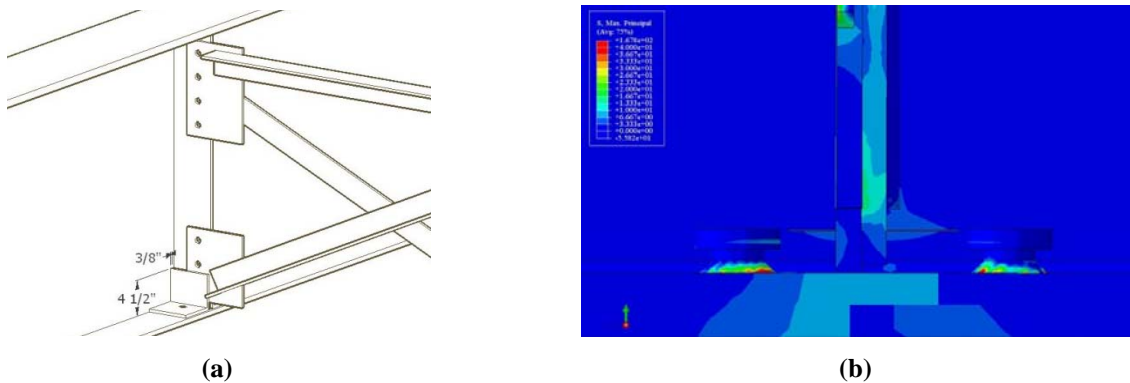


Figure 14. Retrofit measure 5: (a) Schematic of bolted stiffener-to-flange double angles modeled; (b) Maximum principal stress contour plot showing welded bolts at inside face of flange.

Retrofit 3: Transverse Back-up Stiffeners

Retrofit 3 was studied analytically, and two different back-up stiffener geometries were considered. The first was a full-depth back-up stiffener welded to the web, with bearing interaction between the stiffener and the top and bottom flanges_(test), which is shown in Figure 11. In the simulations, bearing was achieved by placing a hard contact interaction between the flanges_(test) and the stiffener. When comparing models that are unretrofitted with a 102-mm (4-in.) horseshoe-shaped crack and an 203-mm (8-in.) horizontal crack versus models that have the same crack configuration and are retrofitted with a full back-up stiffener, it was found that HSS1 decreased by 85% and HSS2 decreased by 60% after the retrofit. It is interesting, too, that if the stiffener was added before cracks formed (i.e., used as a preventative measure), HSS1 values decreased by 13%, but HSS2 increased by a factor of 11.

The second back-up stiffener considered was partial depth [305 mm (12 in.)] and was welded to the web with a hard contact placed between the bottom flange_(test) and the transverse stiffener. This second configuration can be seen in Figure 12. Comparing a cracked, unretrofitted simulation to a cracked, retrofitted simulation with a partial depth stiffener, it was found that HSS1 and HSS2 decreased by 76% and 36%, respectively, after the retrofit.

The stress in the bottom web gap_(test) was allowed to transfer to the backup stiffeners in both configurations. Although HSS1 and HSS2 saw a slightly greater stress reduction with the full depth stiffener as compared to the partial depth stiffener, it should be noted that a localized high area of stress occurred in the weld along the full depth stiffener near the top flange_(test), which did not occur in the partial depth stiffener.

Retrofit measure 4: Composite Block

Retrofit 4 was studied analytically on a cracked model. The crack was modeled explicitly as having a length of 64 mm (2.5 in.), and was located 17 mm (0.65 in.) below the connection stiffener weld. A 127 × 114 × 114-mm (5×4.5×4.5-in.) composite block was designed to fill the entire web gap region, as shown in Figure 13. Tie constraints were used to attach the composite block to the surrounding steel members in the web gap region. The modulus of elasticity of the composite block was varied from 34,500 to 68,950 MPa (5,000 to 10,000 ksi) to evaluate which most effectively reduced the stress in the bottom web gap, and to test the sensitivity of the stress in the web gap region to the stiffness of the CFRP material. It was found that varying the modulus of elasticity changed the HSS values in the steel substrate by less than 0.5%.

Parts made out of composite materials can be manufactured to have different sizes and shapes, and tailored to suit a given geometric configuration. The stress field in Figure 13b shows that significant stresses remained in the steel substrate at the weld between the cross brace and the connection plate after the composite block was in place. This deficiency could be addressed by manufacturing the composite block to extend over the cross-brace-to-gusset weld. Despite the high stresses at the cross-brace-to-gusset weld, the maximum HSS1 in the region directly covered by the CFRP material was reduced by 93%.

Retrofit measure 5: Bolted Stiffener-to-Flange Angles

Retrofit measure 5, studied analytically, consisted of two angles bolted to the bottom flange_(test) and welded to the connection stiffener with geometry as shown in Figure 14a. This retrofit in an actual bridge would often require drilling through the concrete deck to install the bolts, which is not a simple solution. To avoid drilling through the deck, bolts or studs may instead be welded to the inside face of the top flange_(bridge). This retrofit was applied in a simulation with a 64-mm (2.5-in.) crack, modeled explicitly, which was placed 17 mm (0.7 in.) below the connection stiffener-to-web weld. It was found that HSS1 decreased by 95% in the web gap region after application of this retrofit, but a new fatigue prone detail was introduced at the stud weld. This phenomenon can be noted in Figure 14b.

Retrofit measure 6: Bolted Web-to-Stiffener Angles and Backing Plate

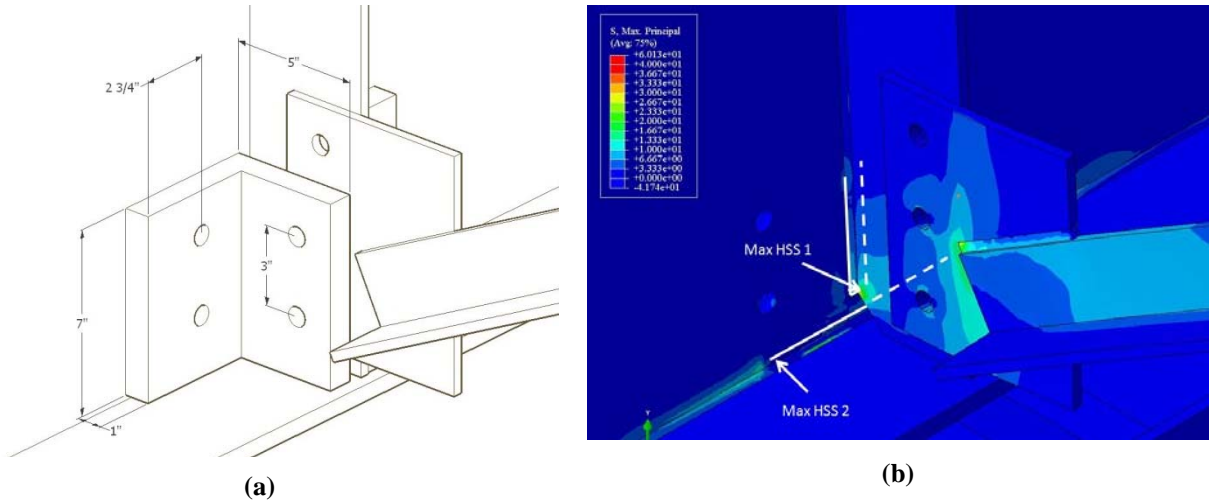
Retrofit measure 6 was studied both analytically and experimentally. This retrofit measure consists of bolting two angles to the web and connection plate, one on each side of the connection plate (Figure 15a; Figure 15c). A backing plate was also bolted to the fascia side of the web to distribute stress away from the bottom web gap_(test) (Figure 16a; Figure 16c). As discussed in the following, thicknesses of the back-to-back steel angles and the back plate were varied to investigate the impact of the stiffness of the structural components on the stresses in the web gap area. In the simulations, all parts were connected through 19-mm (0.75-in.) diameter A325 bolts. Shims were used on both sides of the connection plate to avoid interferences with the welds.

L6×6×3/4 angles and a 457-mm×203-mm×19-mm (18-in.×8-in.×0.75-in.) backing plate were modeled to reflect the dimensions of the retrofit elements used in the physical simulations. In this model, there was a 102-mm (4-in.) horseshoe-shaped crack and a 203-mm (8-in.) horizontal crack in the bottom web gap_(test), dimensions that were consistent with the crack lengths achieved in the physical simulation of the specimen before it was retrofitted. Stresses in the web gap region decreased by 98% for HSS1 and 91% for HSS2 after application of retrofit method 6, compared with the unretrofitted case with a 102-mm (4-in.) horseshoe-shaped crack and a 203-mm (8-in.) horizontal crack. Maximum principal stress contours on the interior of the girder can be seen in Figure 15b, and maximum principal stresses in the web under the backing plate are presented in Figure 16b.

The angle thickness, backing plate thickness, and the backing plate length were varied to determine the effect of the retrofit dimensions. The thicknesses of the members were varied from 6 to 25 mm (0.25 to 1.0 in.), and the length of the backing plate was varied from 3045 to 914 mm (12 to 36 in.). Models in which the angle and back plate thicknesses were 25 mm (1 in.) were designated as a *stiff (s)* combination. When both thicknesses were 13 mm (0.5 in.) the combination was designated as *medium-stiff (m)*. The retrofit was designated *flexible (f)* when both thicknesses were 6-mm (0.25-in.) thick. Other combinations were also considered, in which the backing plate thickness was different from the angle thickness. Computed stresses at the bottom web gap_(test) are listed in Table 2 for various stiffness combinations of retrofit measure 6. When a flexible combination was used, the HSS values in the web gap were found to be more than twice as great as those calculated for a stiff combination, although in all models the stresses were significantly lower than for the model without the retrofit. The variation in HSS between the various stiffnesses of retrofit measure 6 only account for approximately 5% of the maximum unretrofitted HSS.

Table 2. Comparison of HSS values for different retrofit stiffnesses for models with a 102 mm (4 in.) horseshoe crack and a 203 mm (8 in.) horizontal crack; Backplate length held constant at 18 in.

Model Name	HSS1 MPa (ksi)	HSS2 MPa (ksi)
<i>1" thick</i>	23 (3.0)	58 (8.3)
<i>0.5" thick</i>	60 (8.6)	45 (6.5)
<i>0.25" thick</i>	68 (9.8)	55 (8.0)



(c)

Figure 15. Retrofit measure 6: (a) Schematic of retrofit 6 (interior view); (b) Maximum principal stress contours in the web gap region with the angles removed from view; arrows point to point of highest maximum principal stress along HSS Paths 1 and 2. Cracks were modeled with XFEM and contour integrals. (c) Photograph of interior side of girder with stiffener-to-web angle and backing plate retrofit

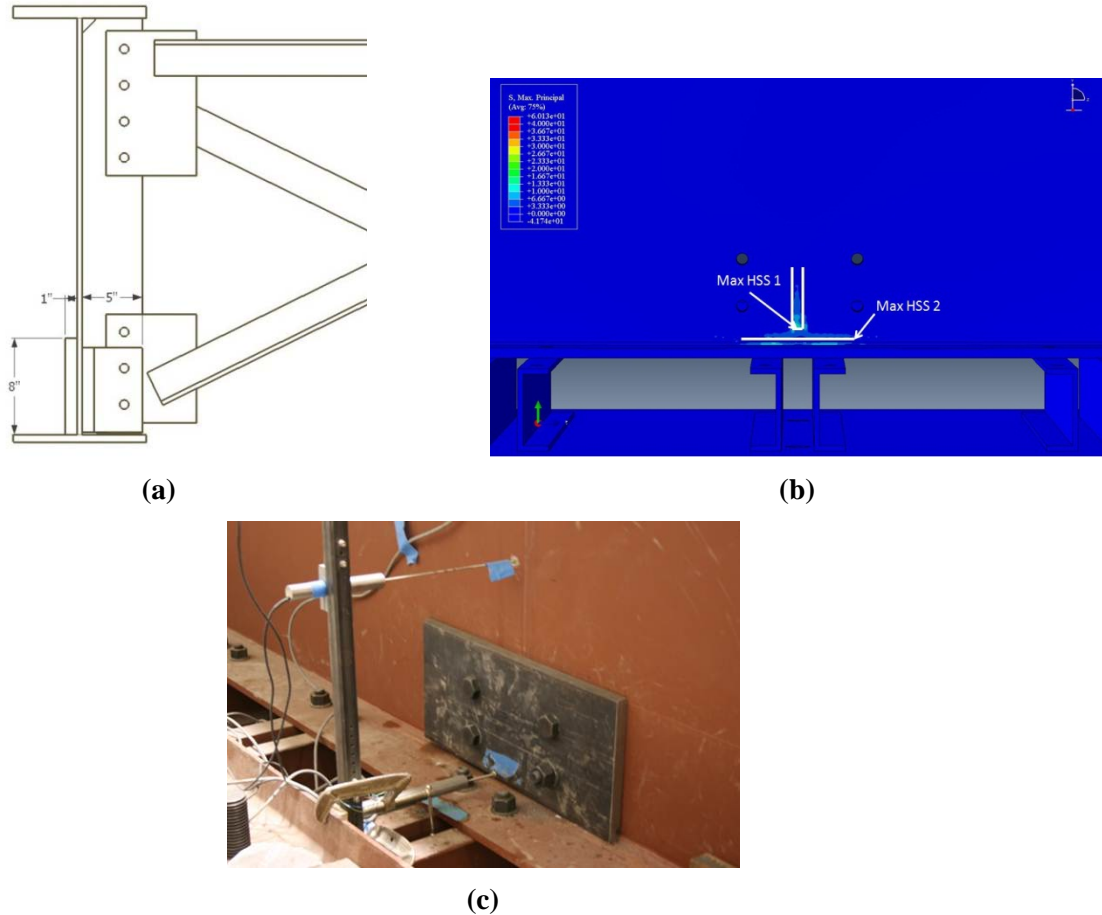


Figure 16. Retrofit measure 6: (a) 457-mm (18-in. long) backing plate on exterior side of web; (b) Maximum principal stress contours on the exterior side of web with the back plate removed from view; arrows point to point of highest maximum principal stress along HSS Paths 1 and 2. Cracks modeled using XFEM and analyzed with contour integrals. (c) Photograph of steel backing plate on fascia side of girder.

When comparing the HSS values for each model, it was found that if the backing plate thickness was kept constant at 25 mm (1.0 in.) (the greatest thickness within the range analyzed), the thickness of the angles had a negligible effect on stress. The opposite also held true; when the angle thickness was kept constant at 25 mm (1.0 in.), the calculated HSS was insensitive to the thickness of the backing plate. Therefore, it was found that choosing the stiffest option for the angle, the backing plate, or both would provide the greatest reduction in the computed stress.

The effect of crack length on the effectiveness of retrofit measure 6 was also analyzed by comparing the computed HSS values. In addition to an uncracked configuration, crack lengths studied were 13 mm, 25 mm, and 102 mm ($\frac{1}{2}$ in., 1.0 in., and 4.0 in.) for the horseshoe-shaped crack, and 13 mm, 25 mm, and 203 mm ($\frac{1}{2}$ in., 1 in., and 8 in.) for the horizontal crack. The longest crack in both series, 102 mm and 203 mm (4 in. and 8 in.), for the horseshoe-shaped and horizontal cracks respectively, were not equal because they were chosen to represent actual crack lengths measured in the physical model at the end of the experiment.

The effect of crack length on HSS was as follows. When stiff angles or a stiff back plate was used, the maximum HSS1 occurred when there were no cracks present. If both a stiff angle and plate were used, HSS1 values decreased slightly as the crack length increased, and eventually stabilized.

Figure 18 and 19 show that HSS 2 and the J-Integral exhibited common trends as the horizontal crack lengthened. In both figures, a 25.4-mm (1-in.) thick back plate was applied, while the thickness of the angles was varied. HSS2 increased slightly as the crack lengthened, up to a crack length of 13 mm – 25 mm ($\frac{1}{2}$ in. – 1 in.), at which point stress in the horizontal crack decreased with further increase in crack length. These findings are important because they shed light on the effect of crack growth on stress when the retrofit is implemented. For the crack lengths studied, it was found that configurations with intermediate crack lengths of 25 mm (1.0 in.) at the web-to-bottom flange_(test) weld produced the greatest demands on the retrofit.

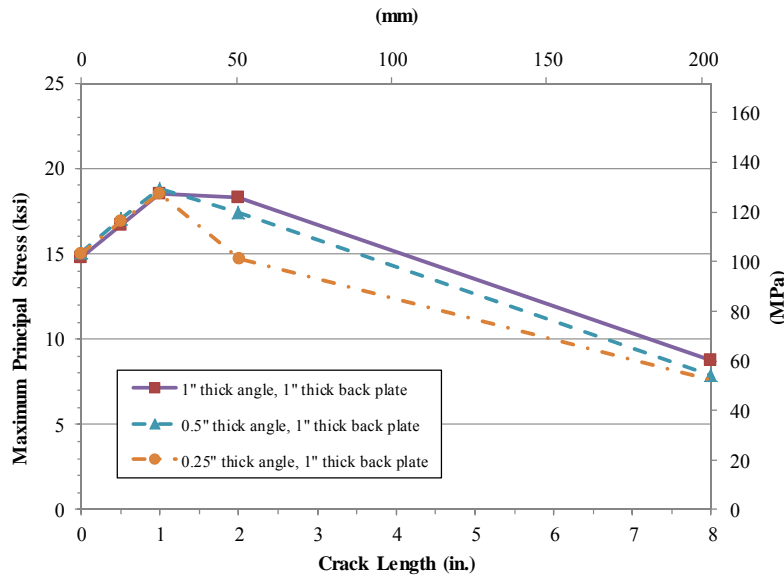


Figure 17. Change in maximum principal stress along HSS path 2 (horizontal web-to-flange weld) as crack length increased.

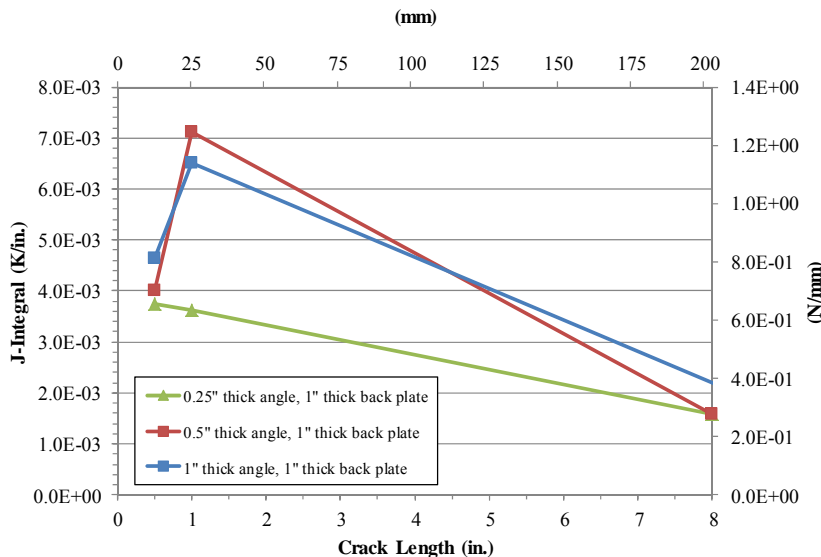


Figure 18. Change in J-Integral for horizontal web-to-flange weld crack as crack length increased.

As mentioned, the bolted web-to-stiffener angles with backing plate retrofit was modeled on cracked and uncracked specimen geometries to examine the effectiveness of the retrofit if used as a preventative

measure. It was seen that HSS 1 and 2 values were similar in magnitude when comparing retrofitted models with various crack lengths to a retrofitted, uncracked model. When 25 mm (1 in.) thick angles and backing plate were used, the uncracked configuration saw an HSS1 value of 60 MPa (8.7 ksi), while the model with a 102-mm (4-in.) crack had an HSS1 value of 38 MPa (5.5 ksi). Similar results were found for HSS2. The web-to-stiffener angles and backing plate retrofit exhibited a high level of stress reduction for both HSS1 and HSS2 in the web gap region for both the uncracked, retrofitted and the cracked, retrofitted scenarios. Therefore, this retrofit shows merit as a preemptive retrofit technique as well as a post-cracking retrofit technique.

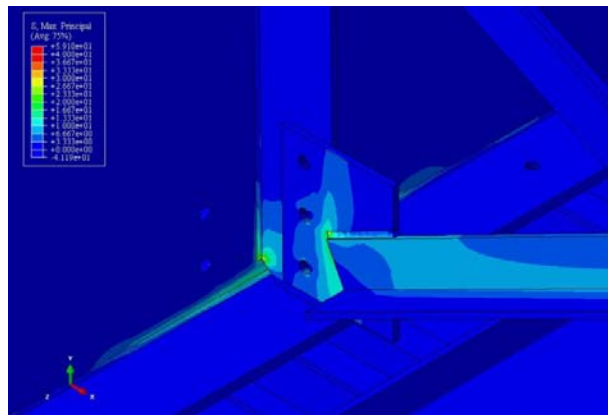


Figure 19. Maximum principal stress contours in an uncracked model with stiff web-to-stiffener angles and backing plate (Retrofit 6) applied.

Conclusions

A study was carried out to evaluate the effectiveness of various retrofit measures for repairing distortion-induced fatigue damage in steel bridge girders. Results from computer and physical simulations have led to the following conclusions:

1. When comparing an uncracked, unretrofitted configuration with an unretrofitted simulation containing a 102 mm (4 in.) horseshoe-shaped crack and a 203 mm (8 in.) long horizontal crack, HSS1 (path parallel to the web-to-stiffener weld) and HSS2 (path parallel to the flange-to-web weld) demands increased by 4.5 \times and 25 \times , respectively, after cracks developed. The areas of high stress moved from the weld toe (uncracked, unretrofitted model) to the tips of the cracks (cracked, unretrofitted model).
2. Computer simulations showed that the web-to-stiffener angle retrofit (retrofit 6) and the composite block (retrofit 4) were the most successful at reducing the calculated stress in the bottom web gap region. Computer simulations of models with retrofit measure 4 (composite block) reduced the HSS1 by 93%. The calculated stress in the bottom web gap for retrofit 6 with a stiff angle and backing plate reduced HSS1 by 98% and HSS2 by 91%, for a configuration with a 102-mm (4-in.) horseshoe-shaped and 203-mm (8-in.) horizontal crack.
3. The web-to-stiffener angles and backing plate retrofit (retrofit 6) exhibited a high level of stress reduction for both HSS1 and HSS2 in the web gap region for both the uncracked, retrofitted and the cracked, retrofitted scenarios. Therefore, this retrofit shows merit as a preemptive retrofit technique as well as a post-cracking retrofit technique.
4. For retrofit measure 6 (stiffener-to-web angles and backing plate), configurations with either the angles or the backing plate as stiff elements (or both as stiff elements) produced the greatest reduction in stress at the web gap region.

5. Drilling of crack-stop holes (retrofit measure 1) at the ends of cracks resulted in negligible reductions in hot spot stress in the web gap region, and the general state of stress in the web gap region remained very significant. The poor performance of this retrofit measure in the computer simulations was corroborated by reinitiation of cracking in the physical specimen after only 39,700 cycles.
6. Installation of a tensioned bolt and plate washer in crack-stop holes (retrofit measure 2) had a negligible effect on stress in the web gap region, and was concluded to be ineffective.
7. The full depth back-up stiffener reduced the stress in the web gap region more than the partial depth back-up stiffener, but corresponded with a very localized stress increase on the fascia side of the web near the top flange_(test).

The primary goal of this study was to evaluate the relative performance of retrofit techniques for distortion-induced fatigue in steel bridge girders. The study showed that the use of angles to attach the connection stiffener to the web with the addition of a backing plate significantly reduced stresses in the web gap region. This is an important finding, because this technique is expected to be inexpensive and easy to install in the field, without significant disruptions to traffic or removal of a concrete deck. Findings regarding the effectiveness of the retrofit technique with various levels of stiffness showed that as long as one of the two element types used in the retrofit (angles and backing plate) were chosen to be stiff, the retrofit was insensitive to variations in stiffness in the other element. This implies that this type of retrofit measure may be effective for many bridge configurations with minimal tailoring for the specific bridge in which it is implemented. It should be noted that additional study in this area is warranted and ongoing before implementation is recommended.

Acknowledgements

The authors would like to acknowledge funding provided by the Kansas Department of Transportation's KTRAN program, as well as Transportation Pooled Fund Study TPF-5(189), which includes support from the following State DOTs: CA, FHWA, IA, IL, KS, LA, NJ, NY, OR, PA, TN, WA, WisDOT, and WY.

References

1. Barsom, J.M & Rolfe, S.T. (2006). *Fracture and Fatigue Control in Structures: Application of Fracture Mechanics* Third Edition. ASTM, West Conshohocken, PA.
2. Fisher, J. W., Jian, J., Wagner, D. C., and Yen, B. T. (1990). "Distortion-induced fatigue cracking in steel bridges." *National Cooperative Highway Research Program Report #336*, Transportation Research Board, National Research Council, Washington, D. C.
3. Zhao, Y. & Kim Roddis, W.M. (2007). "Fatigue behavior and retrofit investigation of distortion-induced web gap cracking." *Journal of Bridge Engineering*, 12(6), 737-745.
4. AISC (2005). *Steel Construction Manual*, 13th Edition, American Institute of Steel Construction, Inc., Chicago, IL.
5. Belytschko, T., Gracie, R., Ventura, G. (2009). "A review of extended/generalized finite element methods for material modelling." *Modelling and Simulation in Materials Science and Engineering*, 17(4), 1-24.
6. Bellec, J., Dolbow, J.E. (2003). "A note on enrichment functions for modelling crack nucleation." *Communications in Numerical Methods in Engineering*, 19,921-932.
7. Simulia. (2010). "Classical Fracture and Failure with Abaqus," Web-based course notes.